Topics in Catalysis
https://doi.org/10.1007/s11244-026-02289-y

ORIGINAL PAPER

Effect of Cu-Fe-Co Catalyst Pretreatment in Higher Alcohol Synthesis

Atte Aho[1] · Irina Simakova[1] · Francesco Sandri[1] · Anssi Peuronen[2] · Daniel Lindberg[3,4] · Päivi Mäki-Arvela[1] · Kari Eränen[1] · Mika Lastusaari[2] · Dmitry Yu. Murzin[1]

Accepted: 2 April 2026

Abstract
Higher alcohol synthesis was carried out over a CuFeCoK/SiO_2 catalyst with the focus on catalyst pretreatment methods. These methods consisted of either reduction with hydrogen, or reduction followed by low temperature carburization with CO, all at 300 °C. Furthermore, a third method was applied without any pretreatment of the catalyst. It was found that the pretreatment using both reduction and carburization gave the most active catalyst in terms of CO conversion within the temperature range tested, 225–300 °C. The apparent activation energy for CO conversion was calculated to be ca. 79 kJ/mol for different pretreatment methods. The pretreatments influenced the product distribution in a way that more alkenes were formed with the reduced and carburized catalyst compared to the catalysts pretreated with the other procedures, while the selectivity to CO_2 was the highest for the only reduced catalyst. The highest selectivity (58.5%) to alcohols was achieved with the un-pretreated catalyst although at the lowest CO conversion, being as low as 4.3% at 225 °C. No catalyst deactivation was observed during testing of the catalysts up to 100 h time on stream independent of the pretreatment method. The theoretical equilibrium compositions was calculated for the different pretreatment methods and compared with catalyst characterisation results.

Keywords Higher alcohol synthesis · Multimetallic catalysts · Catalyst pretreatment · Catalyst characterisation

1 Introduction

Higher alcohols have a broad range of applications in the fine chemistry, specialty chemical, pharmaceutical and energy sectors [1–3]. They are defined as alcohols having two or more carbon atoms in the chain [2]. Higher alcohols can be produced in various ways namely, through fermentation of sugars, hydration of alkenes and catalytically through the syngas route [2]. During higher alcohol synthesis from syngas other reactions can also occur, namely, formation of alkanes and alkenes as well as the water gas shift reaction (WGSR), according to the equations below.

$$n \cdot CO + 2n \cdot H_2 \rightarrow C_nH_{2n+1}OH + (n-1) \cdot H_2O \quad \text{alcohols}$$

$$n \cdot CO + (2n+1) \cdot H_2 \rightarrow C_nH_{2n+2} + n \cdot H_2O \quad \text{alkanes}$$

$$n \cdot CO + 2n \cdot H_2 \rightarrow C_nH_{2n} + n \cdot H_2O \quad \text{alkenes}$$

$$CO + H_2O \leftrightarrow CO_2 + H_2 \quad \text{water gas shift reaction}$$

A wide range of heterogeneous catalysts can be applied in the higher alcohol synthesis (HAS) from syngas being typically grouped as four catalyst families, namely, rhodium [4–6], or molybdenum based [7–11], modified methanol synthesis copper catalysts [12–14] as well as modified Fisher-Tropsch catalysts having cobalt or iron as the active metals [2, 15–19]. Among these catalyst families a copper-iron-cobalt catalyst supported on silica and promoted by potassium was investigated in this work due to the lower price of the active

✉ Dmitry Yu. Murzin
dmitry.murzin@abo.fi

1 Laboratory of Industrial Chemistry and Reaction Engineering, Faculty of Science and Engineering, Johan Gadolin Process Chemistry Centre, Åbo Akademi University, Åbo, Finland

2 Intelligent Materials Chemistry Group, Department of Chemistry, University of Turku, Turku, Finland

3 Laboratory of Molecular Science and Engineering, Faculty of Science and Engineering, Åbo Akademi University, Åbo, Finland

4 Department of Chemical and Metallurgical Engineering, Aalto University, Espoo, Finland

Published online: 24 April 2026

metals compared to the other listed above and high activity and selectivity to higher alcohols as reported in the literature [2, 15, 16, 20]. The novelty of the current study relies on the focus of different pretreatment strategies combined with in-dept product analysis and catalyst characterization.

The modified Fischer-Tropsch catalysts for higher alcohol synthesis can be prepared through impregnation with a metal nitrate solution on a support, followed by calcination to achieve supported metal oxides [21, 22]. Prior to HAS the catalysts are usually reduced in hydrogen at elevated temperatures [21–24], but carburization with CO or syngas has also been applied in some cases [15, 16, 25] as it has been reported that carburization with CO or syngas can improve the activity of Fischer-Tropsch catalysts by forming χ-Fe_5C_2 carbide species [26]. The open literature is scarce on reports where different pretreatment methods were systematically evaluated in HAS [27] or furthermore, where the thermodynamic equilibrium composition of multiphase/metallic catalysts is calculated for different gas atmospheres [28].

The catalyst reported in [27] differs from the copper-iron-cobalt supported on silica catalyst utilized in this work in a way that the latter was prepared through co-precipitation of cobalt, copper, zinc and aluminium nitrates. The catalyst, used in [27], was prepared according to the procedure described in [29] exhibiting the molar ratios of 20:40:15:25 in terms of Co, Cu, Zn and Al, respectively. The HAS experiments in [27] were carried out in a tubular reactor at 280 °C, 60 bar with a gas hourly space velocity of 9600 mL h^{-1} g_{cat}^{-1} and the H_2:CO ratio of 1. Prior to testing, the catalyst was reduced at 350 °C for 15 h, resulting in metallic copper particles but not fully reduced cobalt. The reduction treatment was followed by carburization with CO using different procedures all at 280 °C, namely, for 24 and 50 h at atmospheric pressure or 24 h at 20 bar pressure. Furthermore, one experiment was carried out without carburizing the catalyst after the reduction. It was reported [27] that the only reduced catalyst with metallic copper and cobalt oxide present showed a higher initial activity in CO conversion compared to the carburized catalysts. The same, only reduced, catalyst displayed strong deactivation during the first 10 h of testing, which the authors [27] attributed to modification of the catalyst surface in the presence of syngas through cobalt enrichment and cobalt carbide formation. The CO treated catalysts exhibited also initial deactivation but to a lesser extent. The product distribution was significantly affected by catalyst pretreatment. The only reduced catalyst produced linear hydrocarbons, including methane, with a selectivity of over 65%, while the CO treated catalysts had selectivity to linear hydrocarbons as low as 43.1%. The CO treatment at 20 bar resulted in a significantly improved alcohol selectivity of 36.9%, compared to 21.6% for the reduced only catalyst. The CO conversion in [27] was in the range of 2.5% to 5.7% at 35 h time on stream, it should be noted that CO conversion levels can strongly influence the product distribution as recently reported [15].

In this work the influence of catalyst pretreatment strategies, including absence of pretreatment, reduction alone as well as reduction followed by low temperature carburization using CO at 300 °C, on the activity, stability and selectivity in higher alcohol synthesis using an affordable in-house prepared $CuFeCoK/SiO_2$ catalyst was studied. The testing was carried out at different reaction temperatures (225–300 °C) with in-dept online analysis of gaseous products and detailed off-line liquid analysis. Furthermore, the fresh and spent catalysts were characterized by various techniques and the results compared with theoretical thermodynamic equilibrium compositions of the multimetallic catalyst particles.

2 Experimental

2.1 Catalyst Preparation

The preparation of the $11CuFeCoK/SiO_2$ catalyst used in this work has been described in details elsewhere [16]. Shortly, the catalyst was prepared through incipient wetness impregnation of an aqueous solution of metal nitrates onto silica (Davisil, Sigma Aldrich). The catalyst contained 6 wt% Cu, 4wt.% Fe, 0.5 wt% Co, 0.5 wt% K. After the impregnation, the sample was dried in an oven at 100 °C (17 h) and calcined at 450 °C (6 h) in air with a temperature ramp of 2 °C/min in order to decompose the metal nitrates into oxides.

2.2 Calculation of the Catalyst Thermodynamic Equilibrium Composition

The thermodynamic software Factsage [30] was utilized to calculate the thermodynamic equilibrium composition of the catalysts at conditions corresponding to different heat treatment steps. For the calculations, the following thermodynamic databases were used: FactPS (Pure stoichiometric substances, including gas phase), FTOxid (Stoichiometric solid oxides and oxide solid solutions, as well as molten oxide), FSCopp (Copper based metallic compounds and alloys). The mass of predicted solid phases is directly related to the catalyst composition mentioned above.

2.3 Catalyst Characterization

2.3.1 Nitrogen Physisorption

N_2-physisorption to determine the specific surface area and pore volume was performed with a Micromeritics 3Flex instrument. Prior to the measurements the catalyst samples (~100 mg) were dried ex-situ at 180 °C over night and in-situ at 250 °C for 4 h under vacuum. The specific surface area was calculated using the BET equation, the total pore volume was determined by the Horvath-Kawazoe method and the micropore volume using the t-plot method.

2.3.2 CO DRIFTS

CO DRIFTS measurements were performed with a Shimadzu IRTracer-100 spectrometer equipped with a high-temperature environmental chamber and DRIFTS collector (Spectra-Tech Inc.). Gas lines for N_2, H_2 (Woikoski, N50) and CO (Air Liquide, 3.7) were connected to the water-cooled cell. The experiments were carried out by placing a small amount (~50 mg) of the catalyst powder in the sample holder of the cell thereafter the lid of the cell was attached and after a short N_2-flush the cooling of the cell wall was started. The effect of catalyst pretreatment was studied with CO DRIFTS by applying three different pretreatment conditions similar as in the synthesis of higher alcohols but keeping the different conditions for only 30 min each, namely, reduction with hydrogen at 300 °C with and without carburization using CO also at 300 °C, and using a third pretreatment option that included only drying in nitrogen at 300 °C. The gas flow was 10 mL/min in all cases. After the different pretreatments the cell was cooled down to 25 °C in a flow of nitrogen. After reaching the desired temperature a background spectrum was recorded and thereafter the gas composition was changed to contain 10% CO in nitrogen keeping the same 10 mL/min flow. The catalyst surface was saturated with CO for 15 min and thereafter the flow of CO was discontinued. After switching off the flow of CO, the spectra were recorded immediately at 0 min and thereafter at 5, 10, 20 and 30 min.

2.3.3 XPS

X-ray photoelectron spectroscopy (Thermo Fischer Scientific, NEXSA XPS) was used to analyse the active metals on the fresh pretreated and spent catalysts. Al Kα radiation was used for the measurements with a spot size of 400 µm. Si2p (103.5 eV) peak of the silica support material was used as a reference peak to take possible sample charging into account. Peak fitting of the C1s and K2p regions was done using the XPSPeak4.1 software after taking the Shirley background into account.

2.3.4 Powder XRD

The powder X-ray diffraction data were collected with Malvern PANalytical Aeris Research Edition diffractometer, equipped with PIXcel1D detector, by using Cu $K_{\alpha1,\alpha2}$ radiation (40 kV, 7.5 mA). The samples were prepared onto Si zero-background disc and were rotated at 60 rpm during the data collection. Pulse Height Discrimination (PHD) settings of 7.8 kV for the low and 11.3 kV for the high limit to alleviate issues arising from X-ray fluorescence due to Cu X-ray source and presence of Fe and small amount of Co in the samples. The phase identification was done within HighScore Plus v4.9 software [31] using PDF-4 + database [32].

2.3.5 Transmission Electron Spectroscopy

The different catalysts were analysed by transmission electron microscopy (TEM, Jeol JEM-1400Plus) equipped with an 11 Mpix OsisQuemesa bottom-mounted camera for 120 kV accelerating voltage, for a visual representation. The catalyst samples were dispersed in ethanol and after ultrasonication a drop (5 µL) of the dispersion was deposited onto a 200 mesh copper grid with a micropipette.

2.4 Reactor Set-up and Experimental Procedure

The reactor set-up consisted of a stainless-steel reactor tube with an inner diameter of 6 mm and a total length of 35 cm. The reactor tube was placed in an aluminium block inside the oven (Carbolite) to ensure better heat transfer. The temperature of the oven and the catalyst bed were monitored by K-type thermocouples. The gas flows of hydrogen (Woikoski N50), carbon monoxide (Air Liquide 3.7) and nitrogen (Woikoski N50) were controlled by the Brooks Instrument mass flow controllers (MFC). Nitrogen was used as an internal standard in the flow calculations. The pressure in the set-up was controlled with a backpressure regulator (Equilibar). Downstream the regulator, the formed alcohols were condensed at −15 °C and the gases eluting through the condenser were analysed by an on-line GC (HP 6890 Series) equipped with both HP-PLOT-Q and HP-MOLSIV columns as well as TC and FI detectors for separation and analysis of CO, H_2, N_2, C1-C6 alkanes and C2-C6 alkenes along with CO_2. A scheme of the set-up is displayed in Fig. 1.

The reactor tube was filled by packing quartz wool in the bottom followed by glass beads (Sigma, 425–600 µm) to get the catalyst bed approximately to the middle height of the tube. The catalyst (0.5 g, 125–250 µm) was diluted with the equal amount of the glass beads and finally the

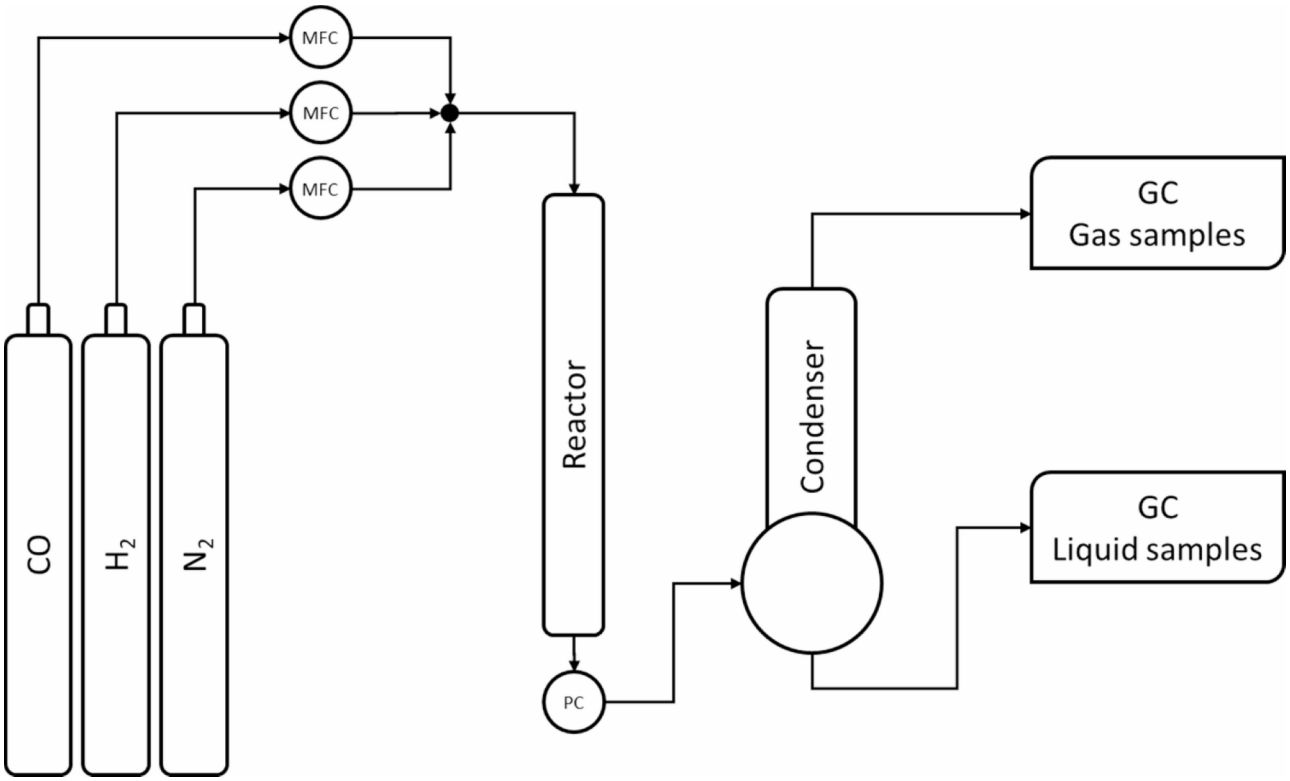

Fig. 1 Reactor set-up scheme

remaining part of the tube was filled with glass beads. The Weisz-Prater (W-P) criterion was calculated to be $1.6 \cdot 10^{-3}$ at the highest reaction temperature (300 °C) and full CO conversion. The low value of the W-P criterion indicates that the pore diffusion limitations can be considered negligible under the tested reaction conditions. Quartz wool was packed between the beds to avoid mixing of the layers.

After filling the reactor tube and placing it in the aluminium block, the tube was attached to the set-up. Thereafter, the set-up was pressurized with nitrogen and carefully checked for possible leakages. When it was ensured that no leakage was present, the pressure was released to atmospheric pressure. Prior to starting the catalyst testing, the catalyst was pretreated by different procedures. A standard pretreatment used in our previous research [5, 15, 16] consisted of reduction for 3 h in 10 mL/min (STP) hydrogen flow followed by carburization for 3 h with 10 mL/min (STP) CO flow at 300 °C, the used gases were not mixed with nitrogen. The reduction temperature of 300 °C was selected based on the temperature programmed reduction analysis reported in [16] where the same catalyst was used. Pretreatments by only reduction at 300 °C and only drying were also applied in the current work. After the pretreatment the gas was switched to nitrogen and the temperature was lowered to 225 °C. Testing of the pretreated catalysts was started at 225 °C by feeding a gas mixture containing 6% nitrogen, as an internal standard for calculating the eluting gas flow composition, as well as hydrogen and carbon monoxide with a ratio of 2 using the gas hourly space velocity (GHSV) of 2000 mL h^{-1} g_{cat}^{-1}. The pressure was increased to 30 bar after flushing the reactor with the reaction gas mixture for approximately 30 min. Different reaction temperatures were tested namely, 225, 250, 275 and 300 °C, each temperature was kept for 24 h with continuous on-line analysis of the gases and collecting one liquid sample at each temperature.

Selectivity to different gas phase products was calculated with the equation

$$S_{x,i} = \frac{n_x \cdot \dot{V}_{x,i}}{\dot{V}_{CO,0} - \dot{V}_{CO,i}} 100\%$$

where n_x is the number of carbon atoms in the product x and $\dot{V}_{x,i}$ is the volumetric flow of the product. The denominator is the converted flow of CO. Selectivity to the liquid phase products is calculated as a difference between 100% and selectivity to the gas phase products. The selectivity to the individual alcohols was calculated with the equation below

$$S_x = S_{liquid} \cdot \frac{n_x \cdot C_x}{\sum_{x=1}^{x=10} n_x \cdot C_x}$$

Table 1 The equilibrium composition of the catalyst after different thermal treatments

Treatment step	Temperature (°C)	Gas composition	Equilibrium phases
Calcination (1)	450	Air	$KFeO_2$ (1.63 g) CuO (5.85 g) $Cu_{0.71}Co_{0.29}Fe_2O_4$ (Spinel, 7.00 g)
Reduction (2)	300	H_2	KOH (0.72 g) Cu (FCC-A1, 6.00 g) $Fe_{0.895}Co_{0.105}$ (BCC-A2, 4.50 g)
Carburization (3)	300	CO	K_2CO_3 (0.88 g) Cu (FCC-A1, 5.64 g) Fe_3O_4 (Magnetite/Spinel#1, 3.35 g) $Cu_{0.4}Co_{0.6}Fe_2O_4$ (Spinel#2, 3.35 g) C (graphite, in excess)
HAS (30 bar)	225	H_2:CO 2:1 (molar ratio)	K_2CO_3 (0.88 g) Cu (FCC-A1, 5.61 g) Fe_3O_4 (Magnetite/Spinel#1, 3.27 g) $Cu_{0.42}Co_{0.58}Fe_2O_4$ (Spinel#2, 3.47 g) C (graphite, in excess)
HAS (30 bar)	250	H_2:CO 2:1 (molar ratio)	K_2CO_3 (0.88 g) Cu (FCC-A1, 5.61 g) Fe_3O_4 (Magnetite/Spinel#1, 3.29 g) $Cu_{0.42}Co_{0.58}Fe_2O_4$ (Spinel#2, 3.44 g) C (graphite, in excess)
HAS (30 bar)	275	H_2:CO 2:1 (molar ratio)	K_2CO_3 (0.88 g) Cu (FCC-A1, 5.62 g) Fe_3O_4 (Magnetite/Spinel#1, 3.31 g) $Cu_{0.41}Co_{0.59}Fe_2O_4$ (Spinel#2, 3.42 g) C (graphite, in excess)
HAS (30 bar)	300	H_2:CO 2:1 (molar ratio)	K_2CO_3 (0.88 g) Cu (FCC-A1, 5.63 g) Fe_3O_4 (Magnetite/Spinel#1, 3.32 g) $Cu_{0.41}Co_{0.59}Fe_2O_4$ (Spinel#2, 3.39 g) C (graphite, in excess)

where S_{liquid} is the selectivity to the liquid products, n_x is the number of carbon atoms in the alcohol x, C_x is the molar concentration of the alcohol in the liquid sample. The collected liquid product was analysed by GC (HP 6890 Series). Separation of the alcohols was done in a FFAP (Agilent, 122–3262) column using the following temperature program, 2 min at 50 °C, heating to 220 °C with 5 °C/min and holding for 10 min. The flame ionization detector was calibrated for linear primary alcohols starting from methanol all the way up to 1-decanol.

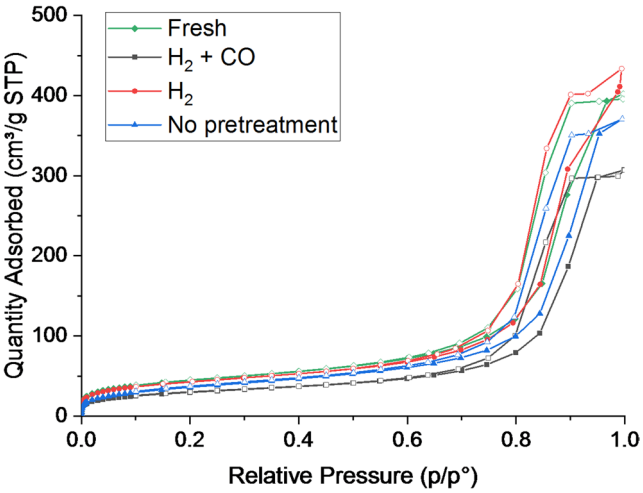

Fig. 2 Nitrogen adsorption/desorption isotherms for the fresh and spent catalyst samples

3 Results and Discussion

3.1 Catalyst Characterization Results

3.1.1 Thermodynamic Equilibrium Composition of the Catalysts

Based on the thermodynamic equilibrium calculations, potassium is stable as either $KFeO_2$, KOH or K_2CO_3, whereas copper is stable as either CuO, metallic Cu or incorporated in an oxide solid solution with the spinel structure also containing Co and Fe. Iron occurs either as $KFeO_2$, Fe_3O_4 (Magnetite, spinel structure), a Cu-Co-Fe oxide solid solution with the spinel structure, or a Fe-Co alloy. Based on the calculations, solid carbon is predicted to precipitate under carburization or high-pressure conditions. The equilibrium composition of the catalyst after different thermal treatments is listed in Table 1 based on a 100 g sample size.

Based on previous works [15, 20] the theoretically calculated equilibrium composition fits fairly well with XRD data reported in the literature, showing the presence of both metallic copper and its oxide as well as a copper-iron spinel, whereas the absence of cobalt in the spinel is most likely due to the low concentration of cobalt in those samples.

3.1.2 Nitrogen Physisorption Results

The specific surface area and the pore volume were determined by nitrogen physisorption for the fresh catalyst sample as well as for the spent catalysts using different pretreatment procedures. The nitrogen adsorption/desorption isotherms are shown in Fig. 2 while the specific surface area calculated with the BET equation, total pore volume

(Horvath-Kawasoe), micropore volume (t-plot) and mesopore volume (by difference) are listed in Table 2.

The specific surface areas for the different spent catalysts are slightly lower than for the fresh, un-pretreated, catalyst. The mesopore volume listed in Table 2 decreases similarly to the specific surface area and the decrease of the specific surface area could be a result of blockage of the mesopores. Potential formation of coke was not further investigated in this work.

3.1.3 CO DRIFTS Results

Figure 3 shows the DRIFTS spectra during 0–15 min CO adsorption and 0–30 min CO desorption, i.e. flushing with nitrogen, for the H_2 + CO pretreated and the catalyst without pretreatment. The CO DRIFTS for the reduced catalyst was previously reported in [16].

The DRIFTS spectra shown in Fig. 3 and in ref [16]. are all very similar independently of the catalyst pretreatment method. During CO adsorption the spectral bands at 2171 and 2119 cm^{-1} are visible, being most likely due to gas phase CO [33] as they disappear during flushing with nitrogen. Interestingly, no bands at all are visible after only 10 min of flushing with nitrogen, which is an indication that the catalyst, independent of the pretreatment method, is not able to adsorb CO strongly enough to be analysed using CO DRIFTS at 25 °C. It has been reported that CO can be linearly adsorbed on Cu^+ sites forming a Cu^+-carbonyl bond, visible at 2120–2136 cm^{-1} [34, 35]. CO can also be weakly adsorbed on highly dispersed metallic copper particles at the same frequency as the Cu^+-CO [35].

3.1.4 XPS Results

Figure 4 shows the survey spectrum of the H_2+CO pretreated catalyst. Clear signals for Si2p and Si2s, C1s, O1s and Cu2p are visible in the spectrum and less visible for the Fe2p peaks. High-resolution spectra for the Cu2p region and Fe2p regions for the pretreated and spent catalysts are shown in Figs. 5 and 6.

Table 2 Specific surface area pore volume (V_p), micropore volume (V_{micro}) and mesopore volume (V_{meso})

Catalyst	BET area (m^2/g)	V_p (cm^3/g)	V_{micro} (cm^3/g)	V_{meso} (cm^3/g)
Fresh	159	0.62	0.01	0.61
H_2+CO	107	0.48	0.00	0.48
H_2	148	0.63	0.01	0.62
No pretreatment	133	0.57	0.00	0.57

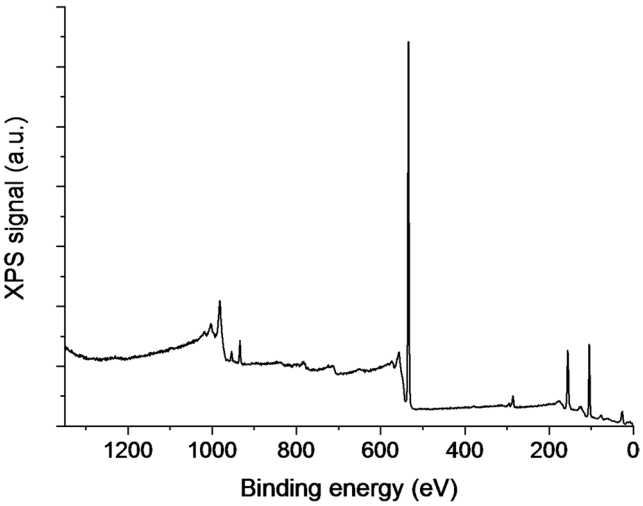

Fig. 4 Survey spectrum of the fresh H_2+CO pretreated catalyst

The high-resolution spectra of the Cu2p region show the $Cu2p_{3/2}$ and $Cu2p_{1/2}$ peaks with a spin orbit splitting binding energy value of 19.75 eV. The Cu2p region of the pretreated catalysts differs from the spent catalysts in a way that the satellite peak at ca. 940–945 eV is clearly visible for the catalyst without any pretreatment and the reduced catalyst while for the H_2 + CO pretreated catalyst it is completely absent. The same satellite peak for the spent catalysts is less pronounced. The main Cu2p3/2 peak is at 932.5–932.9 eV for all catalysts analysed. The strong satellite peak in the catalyst without any pretreatment is a clear indication that CuO is present in this sample, as expected and based on the calculated thermodynamic equilibrium composition of the catalysts reported above, while the absence of the satellite peak indicates, due to the similarities of the main

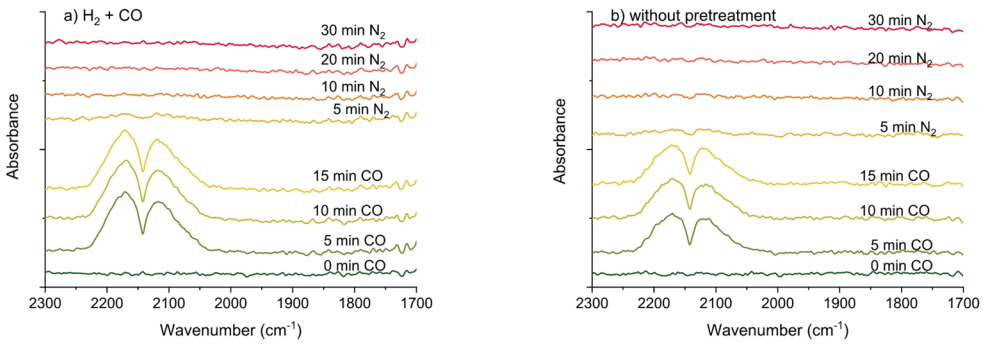

Fig. 3 CO DRIFTS for catalysts treated by (**a**) H_2+CO and (**b**) without any pretreatment

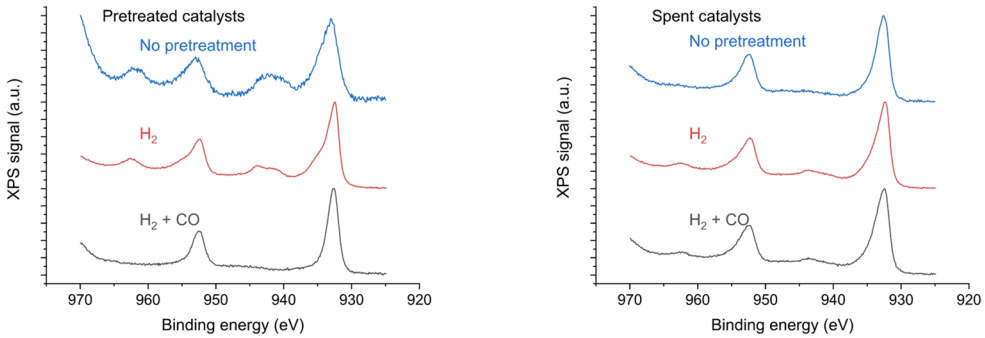

Fig. 5 Cu2p region of XPS spectra for the pretreated (left) and spent (right) catalysts

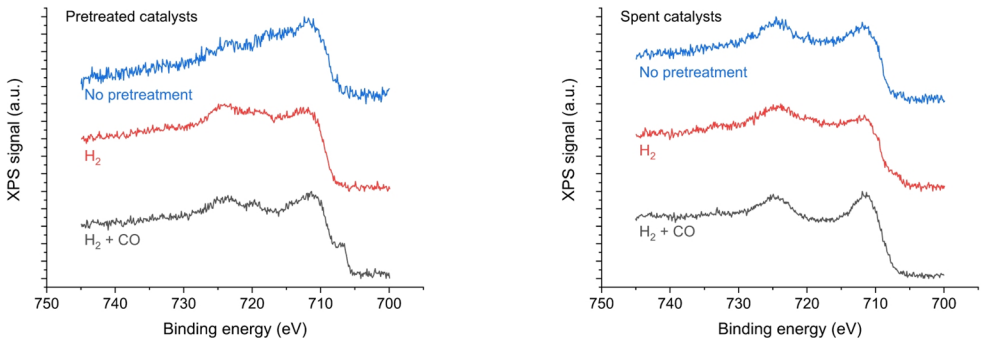

Fig. 6 Fe2p region of XPS spectra for the pretreated (left) and spent (right) catalysts

peak position, that copper is present either as Cu^0 or Cu_2O [36]. According to the thermodynamic calculations of the equilibrium composition the copper of the reduced catalyst should be present in its metallic form. However, the reduced catalyst was previously analysed by XRD [20] where both metallic copper as well as Cu_2O together with iron oxides fitted the data. In a previous paper [20] the fresh catalyst was characterized by temperature programmed reduction exhibiting three peaks at 284 °C, 328 °C and 543 °C. The reduction peak at < 300 °C was assigned to reduction of highly dispersed CuO, the second one > 300 °C as the reduction of larger CuO particles and the last peak as the reduction of Fe according to refs [15, 37, 38]. In this work for the different pretreatments methods, the reduction temperature was 300 °C in all cases which could explain the possible existence of copper oxides. Further characterization of the spent catalysts was performed by XRD and is reported in a later section of the article.

High-resolution spectra of the Fe2p region of the different catalysts are shown in Fig. 6.

Compared to copper there is a bigger difference between the binding energy for metallic iron and different iron oxides. Typically metallic iron shows a peak at approximately 707 eV and different oxides at 2 to 3 eV higher than that [39]. In Fig. 6 most of the main peaks are located at binding energies higher than 710 eV indicating that the iron in all catalysts is present as iron oxide, an exception can be seen for the H_2 + CO pretreated catalyst where a small shoulder is visible at 706.8 eV which can be considered as a signal of the presence of metallic iron also in this catalyst [39, 40]. It has been reported that iron carbides are active in HAS [19]. The binding energy for iron carbide is typically reported to be in the range of 706–708 eV [19, 41] similarly as for metallic iron, although claims of significantly lower ranges for the binding energy have also been reported [42]. In order to verify the presence of iron or other metal carbides, the C1s region should be analysed with a distinct peak located at significantly lower binding energy than the C-C peak at 284.8 eV namely at around 283 eV [27, 43]. In the current catalysts samples no peak at 283 eV was observed indicating the most likely absence of carbides in the catalysts. The C1s region of the reduced and CO treated catalyst, with the peaks assigned to different carbon bonds according to [43], including the K2p, fitted with a spin-orbit splitting of 2.8 eV [44], is shown in Fig. 7 as an example of the absence of the carbide peak. Prior to peak fitting the Shirley background was considered.

3.1.5 XRD Results

The collected XRD patterns of the spent, after HAS, catalysts without any pretreatment and the reduced one are displayed in Fig. 8 both showing the amorphous features of the silica support (Davisil). The most significant peaks in the spent catalyst without any pretreatment are 26.6°, 36.4°, 43.3°, 50.3° and 74.0° 2θ. These correspond well to metallic Cu^0 phase (PDF 00–004-0836), but can also be indicative of mixtures of Cu, Co, and Fe metals. A broad peak at 36.4° accompanied by a broad feature at 61.9° can indicate the presence of Cu_2O (PDF 03–065-3288). The sharp

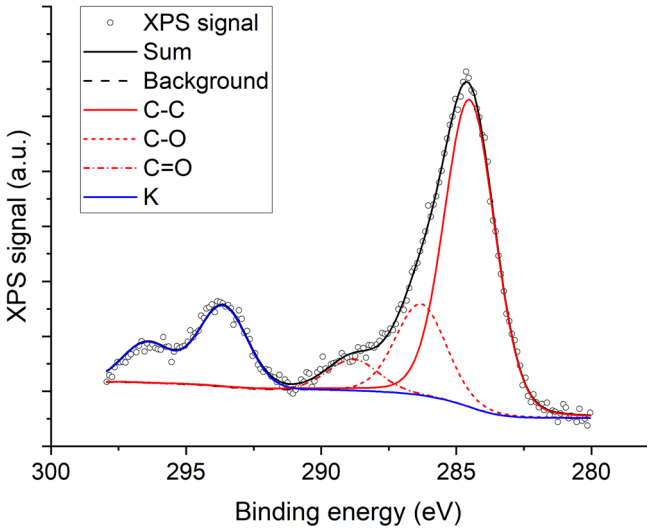

Fig. 7 C1s and K2p regions of XPS spectrum of the H_2 and CO pretreated catalyst

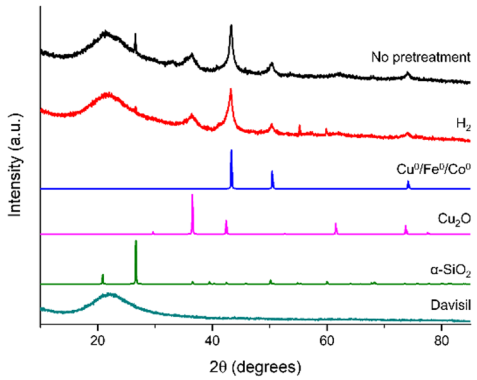

Fig. 8 XRD patterns of spent catalyst without any pretreatment and spent reduced catalyst compared to the crystalline phases found in the literature (Davisil is from self-recorded data)

peak at 26.6° fits well with the main peak of quartz, but its formation is unlikely due to the rather low temperatures to which the sample is subjected and therefore is most likely observed as a contaminant originating from the quartz wool used between the reactor filling beds. The XRD pattern of the spent reduced catalyst is largely similar to the spent catalyst without any pretreatment, where the most notable difference is small intensity of the 26.6° peak and emergence of two new peaks at 55.2° and 59.9°. These peaks all fit to the quartz phase, the most probable reason for the peaks are due to possible contamination of the samples by the quartz wool used in the reactor.

The authors previously reported XRD patterns for the dried and reduced catalyst prior to HAS and for the spent catalyst after the reduction followed by low temperature carburization after HAS [20]. The XRD pattern for the spent sample in that work [20] is almost identical to the patterns displayed in Fig. 8. However, the catalyst without any pretreatment and the reduced catalysts prior to the HAS showed some differences in a way that a $CuFe_2O_4$ spinel phase and Fe_2O_3 fitted the data for the untreated catalyst while the reduced catalyst XRD pattern fitted data for different metal (M^0) and metal oxide phases [20]. Based on the XRD and XPS results for the fresh and spent catalyst it can be concluded that independent of the pretreatment method applied the spent catalysts shows similar results with the two characterization methods.

3.1.6 TEM Results

Visual representation of the catalyst was done by TEM analysis and is shown in Fig. 9.

The TEM images shown in Fig. 9 display some darker spots that might be the active metals with an approximate size of 20 nm corresponding well to the size (15 nm) obtained in an earlier work with the Scherrer equation [20].

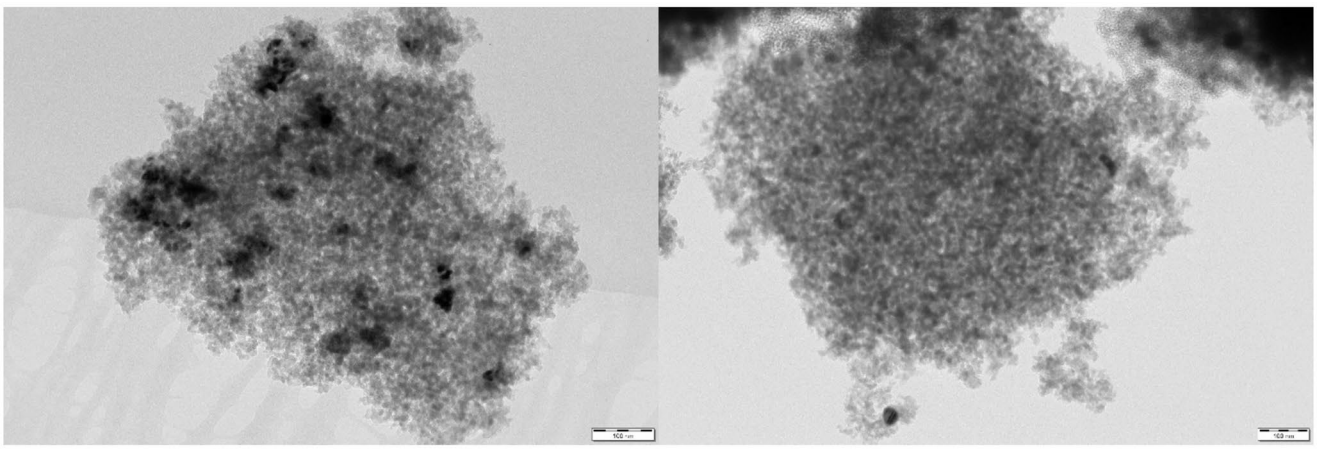

Fig. 9 TEM images of reduced (left) and spent (right) catalysts, the scale bar is 100 nm

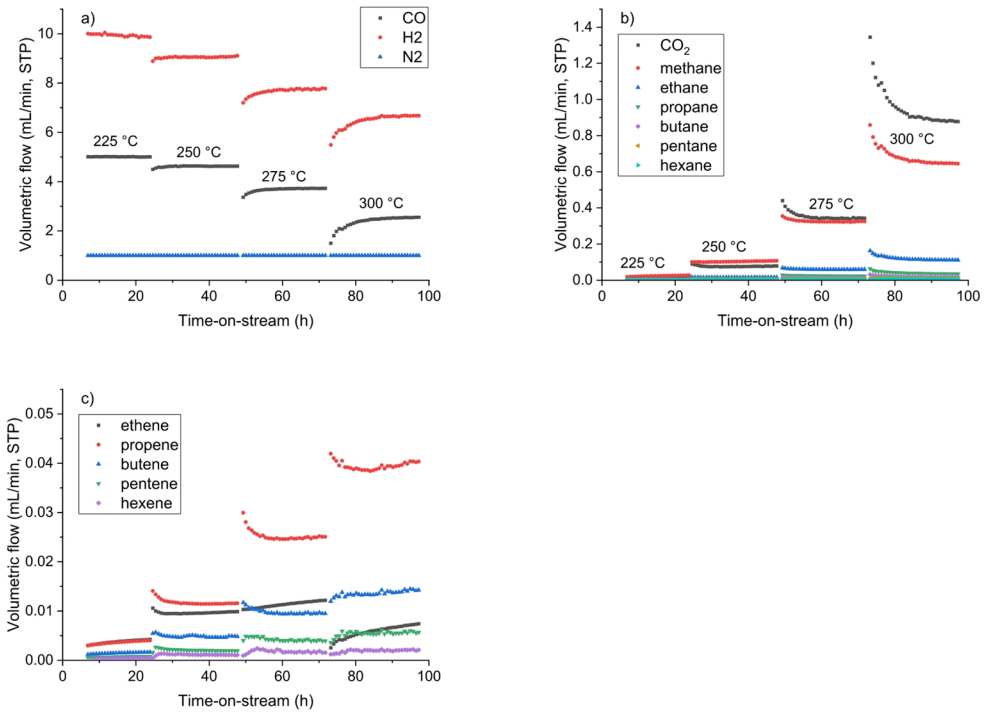

Fig. 10 Volumetric flow of (**a**) CO, H_2 and N_2, **b** CO_2 and C_1-C_6 alkanes and **c** alkenes during an experiment at different reaction temperatures with the untreated $CuFeCoK/SiO_2$ catalyst

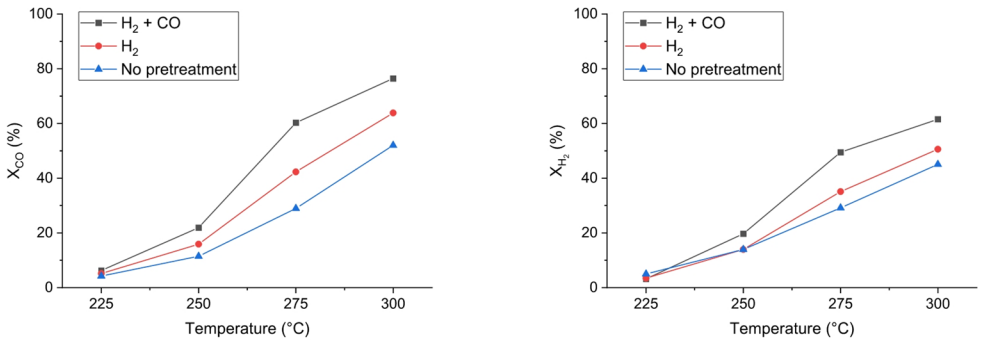

Fig. 11 CO and H_2 conversion as a function of reaction temperature with catalysts having different pretreatment procedures

TEM analysis of copper-iron catalysts supported on silica has been reported [16] to be challenging due to the low contrast between the nanoparticles and the support material probably attributable to the similarity in molar weights.

3.2 Synthesis of Higher Alcohols Results

Figure 10 shows as an example the volumetric flows (mL/min, STP) of the reacting syngas (H_2+CO), the nitrogen flow used as the internal standard, and the gaseous products, CO_2, linear alkanes and alkenes, formed during HAS over the catalyst without any pretreatment. Based on the volumetric flows shown in Fig. 10, the conversion of CO and H_2 and selectivity to the individual gas phase products were calculated and the results are presented and discussed below for the catalysts pretreated using different procedures.

Each temperature displayed in Fig. 10 was kept for 24 h, which was long enough to achieve steady-state conversion of the syngas and fairly constant formation of CO_2 and alkanes. A small increase in the flow of ethene, propene and butene could, however, be observed at the highest reaction temperature. No signs of catalyst deactivation could be detected during testing of the catalysts, pretreated by different methods, for approximately 100 h. Some catalyst deactivation after 500 h of testing using a similar type of catalyst was reported in one earlier study [16]. However, the current paper focuses on the effect of different pretreatment methods of the catalyst and the testing time was not expanded beyond 100 h.

The influence of different pretreatment procedures on the conversion of CO and H_2 as a function of reaction temperature is displayed in Fig. 11.

From Fig. 11 it can be observed that the various pretreatment procedures have a large effect on the conversion of carbon monoxide and hydrogen. Absence of pretreatment resulted in the lowest conversion of CO and H_2 compared to the reduction, while the best pretreatment procedure for achieving high conversion was carried out by first reducing

the catalyst in hydrogen at 300 °C followed by pretreatment in carbon monoxide at the same temperature. It has been reported [26] that carburization with CO increases the CO conversion in FT synthesis with a low alpha iron catalyst as the transformation of iron into χ-Fe_5C_2 is enhanced compared to other pretreatment methods. Iron carbides have been reported to act as the active sites for CO dissociation and chain propagation [45]. Unfortunately, no carbides could be detected with the applied catalyst characterization methods used in this work. Based on the results displayed in Fig. 11 the apparent activation energy for CO conversion was calculated to be between 78.3 and 79.7 kJ/mol which are fairly similar to the previously reported values [15].

Selectivity to the different groups of products namely, alkanes ranging from methane to hexane, alkenes, carbon dioxide and alcohols is displayed in Fig. 12a-d as a function of CO conversion.

Formation of alkanes is not desired in HAS and from Fig. 12a it is observed that by increasing the conversion of CO also the selectivity to these products increases. The lowest selectivity to alkanes is recorded with the only reduced catalyst, while the highest one corresponded to the no pretreatment case. Selectivity to individual alkanes is listed in Table 3 along with selectivity to alkenes, ranging from ethene to hexene, CO_2 and liquid products. The main alkane formed as a by-product is methane. With the reduction and carburization pretreatment the methane selectivity was roughly 20% at all CO conversions levels while for the untreated and reduced catalysts the selectivity started at approximately 10% at the lowest conversion and increased to similar selectivity as for the H_2+CO pretreatment of the catalyst.

The selectivity to alkenes, ethene to hexene, shown in Fig. 12b displays an opposite decreasing trend compared to the alkanes discussed above. Formation of alkenes is not as undesired as formation of alkanes since they could principally be hydrated to the corresponding alcohols over acidic catalysts [46]. However, the reason for the declining selectivity trend is not hydration to the corresponding alcohol but possibly hydrogenation to the corresponding alkane as can be clearly observed as a decrease in ethene selectivity and an increase in ethane selectivity listed in Table 3 although a similar type of catalyst was recently reported to possess some Lewis acidity [16].

Selectivity to CO_2 as a function of CO conversion is plotted in Fig. 12c. The water gas shift reaction forming carbon dioxide and hydrogen is more pronounced at higher CO conversion levels. The only reduced catalyst exhibits a slightly higher selectivity to CO_2 than the pretreated through reduction and carburization as well as without any pretreatment. The current results are in good agreement with those reported in [1, 15] which indicated that relatively large metal particles promotes CO_2 selectivity.

The liquid products selectivity, mainly primary alcohols, for the catalysts with different pretreatment methods as a function of CO conversion is shown in Fig. 12d. The

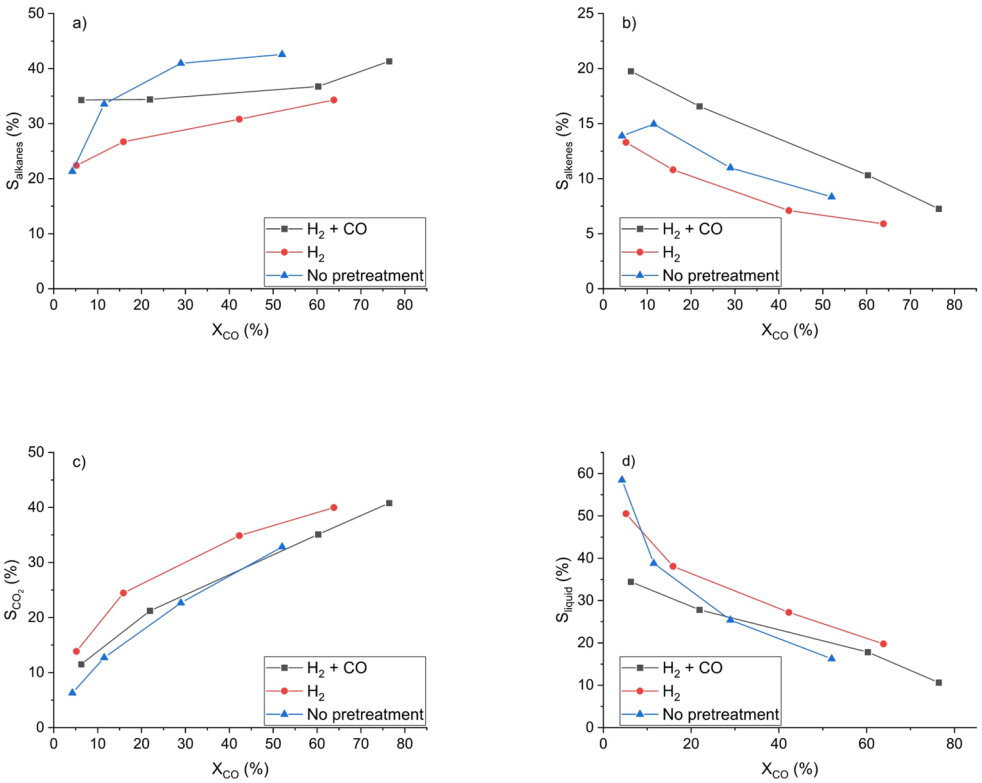

Fig. 12 Selectivity to (**a**) alkanes, **b** alkenes, **c** CO_2, **d** liquid products as a function of CO conversion over catalysts pretreated with different methods

Table 3 Conversion of CO and H_2 as well as selectivity to individual gas phase products including alkanes, alkenes and CO_2 for the tested catalyst pretreatments at different reaction temperatures. Selectivity to liquid products is calculated by the difference

Pretreatment	Temperature	CO	H_2	Methane	Ethane	Propane	Butane	Pentane	Hexane	Ethene	Propene	Butene	Pentene	Hexene	CO_2	Liquid
H_2+CO	225	6.3	3.1	20.1	5.0	4.0	2.7	1.6	0.8	5.8	7.4	3.7	1.8	1.0	11.5	34.4
	250	21.9	19.7	19.3	6.8	3.5	2.4	1.5	0.8	3.2	7.0	3.7	1.8	0.9	21.2	27.8
	275	60.3	49.9	19.9	8.3	3.6	2.4	1.6	1.0	0.8	5.3	2.5	1.2	0.5	35.1	17.8
	300	76.4	61.7	23.7	8.4	3.7	2.5	1.8	1.1	0.3	4.1	1.7	0.8	0.3	40.8	10.6
H_2	225	5.2	3.5	11.3	3.0	3.1	2.4	1.6	1.0	3.8	4.7	2.6	1.4	0.9	13.9	50.5
	250	15.9	14.0	14.0	4.4	3.2	2.4	1.5	1.0	2.3	4.1	2.3	1.2	0.8	24.5	38.1
	275	42.3	35.1	17.0	5.9	3.2	2.3	1.5	1.0	0.8	3.2	1.7	0.9	0.5	34.9	27.2
	300	63.8	50.6	21.0	6.5	2.8	1.9	1.3	0.8	0.3	3.3	1.4	0.7	0.3	40.0	19.8
no pretreatment	225	4.3	5.0	10.8	2.7	2.9	2.3	1.6	1.1	3.5	5.0	2.7	1.6	1.1	6.3	58.5
	250	11.5	14.0	17.4	5.3	4.1	3.2	2.1	1.4	3.2	5.7	3.2	1.7	1.1	12.7	38.8
	275	29.0	29.2	21.4	7.9	4.6	3.4	2.3	1.5	1.5	4.9	2.5	1.3	0.7	22.7	25.4
	300	52.0	45.1	24.0	8.4	4.0	2.9	2.0	1.3	0.5	4.3	2.0	1.0	0.5	32.8	16.3

selectivity shows a decreasing trend with increased CO conversion as also reported earlier [15, 16].

Based on the selectivity to liquid products illustrated in Fig. 12d and the concentrations of the alcohols obtained by GC analysis, the selectivity to individual alcohols was calculated and listed in Table 4. The Anderson-Schulz-Flory (ASF) distribution equation was used to calculate the α-values for ethanol and longer alcohols. Another descriptor also listed in Table 4, namely the β-value, describes the ratio of higher alcohols to methanol weight fractions. The equations for calculating α- and β-values are given elsewhere [15]. The α-values are approximately 0.3 for most pretreatments and reaction conditions, except for the untreated catalyst at 250 °C where it was 0.44. However, the β-value for this alcohol mixture is one of the lowest (2.5) while the same β-value is around 3 and higher for the reduced and H_2 + CO pretreated catalysts. It was not possible, obviously, to collect any liquid sample after 225 °C due to the low CO conversion.

The α- and β-values listed in Table 4 are comparable with the results from the open literature, namely the authors have recently reported [20] average α-values of 0.3 using a similar type of catalysts studied in a more broad parameter space. Another study [15] focusing on the copper-iron ratio of a CuFeCoK/attapulgite catalyst gave α-values of ca. 0.3 in all catalyst configurations but a clear trend was observed for the β-value which was significantly higher (2.57) for iron rich catalysts compared to the copper rich catalyst (1.58). Much higher α-values 0.71–0.81 were reported in the literature [47] for a co-precipitated CuFe catalyst with the lower α-value and a three-dimensionally ordered microporous Cu-Fe catalyst for the higher α-value. The latter catalyst was prepared by a multistep colloidal crystal template method.

Note that the aim of the work was to promote chain growth of the formed alcohols, rather than hydrocarbons even if the catalyst resembles a Fischer-Tropsch catalyst. While a good FT Co-catalyst can produce hydrocarbons with an α-value exceeding 0.9, as illustrated above the α-value in the current work was calculated to be ca. 0.3, fitting nicely with the ASF distribution. If C_{10}^+ or even C_{20}^+ alkanes, alkenes or alcohols with an α-value of 0.5 would be formed, then the analyzed product distribution would be shifted in a way that the main product would have a higher carbon number than reported here. Moreover, selectivity to different products listed in Tables 3 and 4 decreases quite fast to ca. zero. Analysis of hydrocarbons up to C_6 was performed with the on-line GC downstream the condenser operating at −15 °C. The temperature of the condenser was selected to be this low as the partial pressure of neat methanol and ethanol at this temperature is lower than 2 kPa. As the aim of the study was to generate alcohols, capturing them was considered therefore essential for the off-line analysis. Moreover,

Table 4 Selectivity to alcohols, α- and β-values for the tested catalyst pretreatments at different reaction temperatures (°C)

Pretreatment	Temperature	Methanol	Ethanol	Propanol	Butanol	Pentanol	Hexanol	Peptanol	Octanol	Nonanol	Decanol	α	R2	β
H_2+CO	250	5.1	13.1	5.7	3.0	0.7	0.1	0.0	0.0	0.0	0.0	0.33	0.91	2.98
	275	3.4	8.5	3.3	1.7	0.7	0.2	0.0	0.0	0.0	0.0	0.28	0.97	2.84
	300	1.7	5.2	1.9	1.0	0.5	0.2	0.1	0.0	0.0	0.0	0.34	0.99	3.41
H_2	250	5.9	19.1	7.5	4.1	0.7	0.4	0.2	0.1	0.0	0.0	0.32	0.98	3.64
	275	4.8	12.3	5.0	3.3	1.4	0.3	0.1	0.1	0.0	0.0	0.28	0.99	3.10
	300	3.7	9.3	3.3	1.8	1.0	0.4	0.1	0.1	0.0	0.0	0.37	0.99	2.93
no pretreatment	250	8.1	18.1	5.4	3.4	1.4	0.7	1.0	0.3	0.3	0.0	0.44	0.94	2.50
	275	5.3	11.5	4.3	2.7	1.2	0.3	0.0	0.0	0.0	0.0	0.32	0.95	2.54
	300	3.7	7.8	2.7	1.3	0.6	0.2	0.0	0.0	0.0	0.0	0.29	0.96	2.30

the tubing from the reactor to the pressure controller had an inner diameter of roughly 1.5 mm, subsequently if some heavier solid products would have been formed with the current catalyst they would have eventually eluted into the collector from where the liquid samples were withdrawn. Such solids were formed in a current set-up with a catalyst having a significantly higher cobalt loading than used in this work where the cobalt loading was 0.5 wt%. On the contrary, no waxes were detected in this work.

4 Conclusions

Synthesis of higher alcohols was studied using an 11 wt% $CuFeCoK/SiO_2$ catalyst with individual loadings of 6 wt%, 4 wt%, 0.5 wt% and 0.5 wt% for the different metals. The influence of different pretreatment methods prior to the catalytic experiments was carried out by utilizing a catalyst without any pretreatment, a reduced catalyst and a reduced and carburized catalyst. The pretreatment affected the syngas conversion in a way that the untreated catalyst showed a lower conversion of both CO and H_2 at all tested temperatures while the reduced and carburized catalyst displayed the highest conversion. The pretreatment method also influenced the product distribution in a way that higher selectivity towards alkenes was achieved with the reduced and carburized catalyst compared to the catalysts pretreated with the other procedures, while the reduced catalyst showed highest formation of CO_2. The highest selectivity (58.5%) to alcohols was achieved with the un-pretreated catalyst although at the lowest CO conversion it was as low as 4.3% at 225 °C. No signs of catalyst deactivation were observed during testing of the catalysts up to 100 h time on stream independent of the pretreatment method.

Acknowledgements This work is part of the activities of the Johan Gadolin Process Chemistry Centre at Åbo Akademi University. Funding from Business Finland through the SynJet project is greatly acknowledged. Materials research infrastructure/Department of Physics and Astronomy, University of Turku is gratefully acknowledged for the possibility to use their XPS. The catalyst samples were processed and analysed using the TEM at the Electron Microscopy Laboratory, Institute of Biomedicine, University of Turku, which received financial support from Biocenter Finland.

Author Contributions AA, IS, FS, AP, KE, ML contributed to the experimental work. Overall supervision was done by PMA and DYM. AA wrote the main manuscript text. All authors reviewed the manuscript.

Funding Open access funding provided by Åbo Akademi University.

Data Availability the data will be made available upon request.

Declarations

Conflict of interest There are no conflicts of interest to declare.

References

1. Luk HT, Mondelli C, Mitchell S, Siol S, Stewart JA, Curulla Ferré D et al (2018) Role of carbonaceous supports and potassium promoter on higher alcohols synthesis over copper–iron catalysts. ACS Catal Am Chem Soc 8:9604–9618. https://doi.org/10.1021/acscatal.8b02714
2. Luk HT, Mondelli C, Ferré DC, Stewart JA, Pérez-Ramírez J (2017) Status and prospects in higher alcohols synthesis from syngas. Chem Soc Rev Royal Soc Chem 46:1358–1426. https://doi.org/10.1039/C6CS00324A
3. Al Ghatta A, Aravenas RC, Wu Y, Perry JM, Lemus J, Hallett JP (2022) New Biobased Sulfonated Anionic Surfactants Based on the Esterification of Furoic Acid and Fatty Alcohols: A Green Solution for the Replacement of Oil Derivative Surfactants with Superior Proprieties. ACS Sustainable Chem Eng Am Chem Soc 10:8846–8855. https://doi.org/10.1021/acssuschemeng.2c01766
4. Wang R, Cao H, Ma P, Bao J (2024) Maximizing the number of Rh0–Rh+ sites through metal dispersion control for the synthesis of higher alcohols from syngas. J Mater Chem Royal Soc Chem 12:26791–26799. https://doi.org/10.1039/D4TA04890C
5. Lind N, Aho A, Eränen K, Virtanen P, Simakova I, Mäki-Arvela P et al (2024) Transformation of syngas to valuable oxygenated products over Rh-MnOx/SiO2, Rh-Co/ZrO2 and Rh-Cu/ZrO2 catalysts. Appl Catal A:General 683:119852. https://doi.org/10.1016/j.apcata.2024.119852
6. Liu Y, Murata K, Inaba M, Takahara I, Okabe K (2011) Synthesis of ethanol from syngas over Rh/Ce1 – xZrxO2 catalysts. Catal Today 164:308–314. https://doi.org/10.1016/j.cattod.2010.10.087
7. Yang Z, Luo M, Liu Q, Li C, Wang Y, Li H et al (2024) Effect of K and Ni Promoters on Mo2C/Al2O3 Catalyst for Higher Alcohols Synthesis from Syngas. Kinet Catal 65:251–260. https://doi.org/10.1134/S0023158424601189
8. Wang C, Yu H, Lin T, Qi X, Yu F, Zhong L et al (2022) Direct synthesis of higher alcohols from syngas over modified Mo2C catalysts under mild reaction conditions. Catal Sci Technol Royal Soc Chem 12:1697–1708. https://doi.org/10.1039/D1CY02186A
9. ten Have IC, Valle E, Gallo A, Snider JL, Duyar MS, Jaramillo TF (2019) Development of Molybdenum Phosphide Catalysts for Higher Alcohol Synthesis from Syngas by Exploiting Support and Promoter Effects. Energy Technol 7:1801102. https://doi.org/10.1002/ente.201801102
10. Meng S, Zhang T, Xue X, Ding Z, Huang C, Ren P et al (2026) Construction of Mo2C catalyst based on Ni-MOF for synthesis of higher alcohols from syngas. Chem Eng J 528:172167. https://doi.org/10.1016/j.cej.2025.172167
11. Meng S, Gu J, Jiang S, Weng Y, Huang C, Ren P et al (2024) Lignin carbon-initiated Ni/K/Mo2C catalyst for efficient synthesis of higher alcohols from syngas. Chem Eng J 481:148751. https://doi.org/10.1016/j.cej.2024.148751
12. Heracleous E, Liakakou ET, Lappas AA, Lemonidou AA (2013) Investigation of K-promoted Cu-Zn-Al, Cu-X-Al and Cu-Zn-X (X = Cr, Mn) catalysts for carbon monoxide hydrogenation to higher alcohols. Appl Catal A 455:145–154. https://doi.org/10.1016/j.apcata.2013.02.001
13. Hong Z, Wang J, Gao Z, Huang W (2024) Tuning CuO crystallite size by different solvents for higher alcohols synthesis from syngas over CuZnAl catalyst. Int J Hydrog Energy 56:1032–1037. https://doi.org/10.1016/j.ijhydene.2023.12.292
14. Slaa JC, van Ommen JG, Ross JRH (1992) The synthesis of higher alcohols using modified Cu/ZnO/Al2O3 catalysts. Catal Today 15:129–148. https://doi.org/10.1016/0920-5861(92)80125-7
15. Aho A, Lind N, Virtanen P, Mäki-Arvela P, Eränen K, Granroth S et al (2024) Influence of Cu:Fe ratio in synthesis of higher alcohols from syngas over CuFeCoK/attapulgite catalysts. Appl Catal O: Open 193:206972. https://doi.org/10.1016/j.apcato.2024.206972
16. Aho A, Rahman H, Yevdokimova O, Murzin DY, Rebrov E (2025) Synthesis of higher alcohols over K-promoted CuFe/SiO2 catalysts. Catalysis Today 460:115485. https://doi.org/10.1016/j.cattod.2025.115485
17. Xiang Y, Kruse N (2016) Cobalt–copper based catalysts for higher terminal alcohols synthesis via Fischer–Tropsch reaction. J Energy Chem 25:895–906. https://doi.org/10.1016/j.jechem.2016.09.014
18. Xiao K, Bao Z, Qi X, Wang X, Zhong L, Fang K et al (2013) Structural evolution of CuFe bimetallic nanoparticles for higher alcohol synthesis. J Mol Catalysis A: Chem 378:319–25. https://doi.org/10.1016/j.molcata.2013.07.006
19. Xu J, Wei J, Zhang J, Liu N, Ge Q, Sun J (2023) Precisely synergistic synthesis of higher alcohols from syngas over iron carbides. Chem Catalysis 3:100584. https://doi.org/10.1016/j.checat.2023.100584
20. Aho A, Suomalainen M, Peuronen A, Mikkonen HI, Heikkinen N, Mäki-Arvela P et al (2025) Synthesis of higher alcohols from syngas: exploring the parameter space and conceptual process design. Chem Eng Res Design 222:1–14. https://doi.org/10.1016/j.cherd.2025.08.038
21. Yang W, Chen M, Zhou J, Duan Y, An Y, Liu M et al (2020) Preparation and evaluation of highly dispersed HHSS supported Cu-Fe bimetallic catalysts for higher alcohols synthesis from syngas. Appl Catalysis A: Gen 608:117868. https://doi.org/10.1016/j.apcata.2020.117868
22. Gong N, Wu Y, Ma Q, Tan Y (2023) A simple strategy stabilizing for a CuFe/SiO2 catalyst and boosting higher alcohols' synthesis from syngas. Catalysts 13:237. https://doi.org/10.3390/catal13020237
23. Han X, Fang K, Zhou J, Zhao L, Sun Y (2016) Synthesis of higher alcohols over highly dispersed Cu–Fe based catalysts derived from layered double hydroxides. J Colloid Interface Sci 470:162–71. https://doi.org/10.1016/j.jcis.2015.09.062
24. Ge Y, Zou T, Martín AJ, Pérez-Ramírez J (2023) ZrO2-promoted Cu-Co, Cu-Fe and Co-Fe catalysts for higher alcohol synthesis. ACS Catalysis 13:9946–59. https://doi.org/10.1021/acscatal.3c02534
25. Xiao K, Qi X, Bao Z, Wang X, Zhong L, Fang K et al (2013) CuFe, CuCo and CuNi nanoparticles as catalysts for higher alcohol synthesis from syngas: a comparative study. Catal Sci Technol

Royal Soc Chem 3:1591–1602. https://doi.org/10.1039/C3CY00063J
26. Luo M, Hamdeh H, Davis BH (2009) Fischer-Tropsch synthesis: catalyst activation of low alpha iron catalyst. Catal Today 140:127–134. https://doi.org/10.1016/j.cattod.2008.10.004
27. Nebel J, Schmidt S, Pan Q, Lotz K, Kaluza S, Muhler M (2019) On the role of cobalt carbidization in higher alcohol synthesis over hydrotalcite-based Co-Cu catalysts. Chin J Catal 40:1731–1740. https://doi.org/10.1016/S1872-2067(19)63344-9
28. Parmon VN (2013) Stationary phase state of the active component of a solid catalyst being in contact with a reactive fluid of nonequilibrium composition. Dokl Phys Chem 452:200–204. https://doi.org/10.1134/S0012501613090017
29. Anton J, Nebel J, Göbel C, Gabrysch T, Song H, Froese C et al (2016) CO hydrogenation to higher alcohols over Cu–Co-based catalysts derived from hydrotalcite-type precursors. Top Catal 59:1361–1370. https://doi.org/10.1007/s11244-016-0663-2
30. Bale CW, Bélisle E, Chartrand P, Decterov SA, Eriksson G, Gheribi AE et al (2016) FactSage thermochemical software and databases, 2010–2016. Calphad 54:35–53. https://doi.org/10.1016/j.calphad.2016.05.002
31. Degen T, Sadki M, Bron E, König U, Nénert G (2014) The high-score suite. Powder Diffr 29:S13–S18. https://doi.org/10.1017/S0885715614000840
32. Gates-Rector S, Blanton T (2019) The powder diffraction file: a quality materials characterization database. Powder Diffr 34:352–360. https://doi.org/10.1017/S0885715619000812
33. Sonal, Pant KK, Upadhyayula S (2020) An insight into the promotional effect on Fe-Co bimetallic catalyst in the Fischer Tropsch reaction: A DRIFTS study. Fuel 276:118044. https://doi.org/10.1016/j.fuel.2020.118044
34. Hornés A, Bera P, Cámara AL, Gamarra D, Munuera G, Martínez-Arias A (2009) CO-TPR-DRIFTS-MS *in situ* study of CuO/Ce1−*x*Tb*x*O2−*y* (*x*=0, 0.2 and 0.5) catalysts: support effects on redox properties and CO oxidation catalysis. J Catal 268:367–75. https://doi.org/10.1016/j.jcat.2009.10.007
35. Subramanian ND, Kumar CSSR, Watanabe K, Fischer P, Tanaka R, Spivey JJ, The Royal Society of Chemistry (2012) A DRIFTS study of CO adsorption and hydrogenation on Cu-based core–shell nanoparticles. Catal Sci Technol 2:621–31. https://doi.org/10.1039/C2CY00413E
36. Biesinger MC, Lau LWM, Gerson AR, Smart R (2010) Resolving surface chemical states in XPS analysis of first row transition metals, oxides and hydroxides: Sc, Ti, V, Cu and Zn. Appl Surf Sci 257:887–98. https://doi.org/10.1016/j.apsusc.2010.07.086
37. He M, Luo M, Fang P (2006) Characterization of CuO species and thermal solid-solid interaction in CuO/CeO2-Al2O3 catalyst by in-situ XRD, raman spectroscopy and TPR. J Rare Earths 24:188–92. https://doi.org/10.1016/S1002-0721(06)60091-4
38. Khunphonoi R, Khemthong P, Luadthong C, Kuboon S, Kongmark C, Viriya-empikul N et al (2022) Correlating the effect of preparation methods on the structural and magnetic properties, and reducibility of $CuFe_2O_4$ catalysts. RSC Adv 12:15526–33. https://doi.org/10.1039/D2RA01708C
39. Biesinger MC, Payne BP, Grosvenor AP, Lau LWM, Gerson AR, Smart RSC (2011) Resolving surface chemical states in XPS analysis of first row transition metals, oxides and hydroxides: Cr, Mn, Fe, Co and Ni. Appl Surf Sci 257:2717–2730. https://doi.org/10.1016/j.apsusc.2010.10.051
40. Smit E, Groot F, Blume R, Hävecker M, Knop-Gericke A, Weckhuysen BM, The Royal Society of Chemistry (2009) The role of Cu on the reduction behavior and surface properties of Fe-based Fischer–Tropsch catalysts. Phys Chem Chem Phys 12:667–80. https://doi.org/10.1039/B920256K
41. Liu Y, Ma Y, Pu X, Han X, Ye L, Kong L et al (2025) Influence of supports in CuFe-based catalysts for hydrogenation of CO2 to ethanol. Fuel 395:135192. https://doi.org/10.1016/j.fuel.2025.135192
42. Zhu R, Wang K, Xing Y, Li C, Gao X, Ma Q et al (2024) Preparation of Fe-based catalysts from waste biomass as a carbon carrier and its catalytic performance in CO2 hydrogenation. New J Chem 48:9920–30. https://doi.org/10.1039/D4NJ00779D
43. Carbon | XPS Periodic Table - FI [Internet]. [cited 2026 Feb 3]. https://www.thermofisher.com/uk/en/home/materials-science/learning-center/periodic-table/non-metal/carbon.html. Accessed 3 Feb 2026
44. Potassium | Periodic Table - FI [Internet] [cited 2026 Feb 3]. https://www.thermofisher.com/uk/en/home/materials-science/learning-center/periodic-table/alkali-metal/potassium.html. Accessed 3 Feb 2026
45. Zeng Z, Li Z, Guo S, Lv J, Huang S, Wang Y et al (2021) Janus Au–Fe2.2C catalyst for direct conversion of syngas to higher alcohols. ACS Sustain Chem Eng 9:11258–68. https://doi.org/10.1021/acssuschemeng.1c04263
46. Britton RA Direct hydration of ethylene to ethanol [Internet]. 1972 [cited 2025 Apr 16]. https://patents.google.com/patent/US3686334A/en. Accessed 16 Apr 2025
47. Lu Y, Cao B, Yu F, Liu J, Bao Z, Gao J (2014) High selectivity higher alcohols synthesis from syngas over three-dimensionally ordered macroporous Cu-Fe catalysts. ChemCatChem 6:473–8. https://doi.org/10.1002/cctc.201300749